

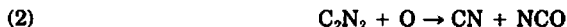
Shock Tube Study of Cyanogen Oxidation Kinetics

MICHEL Y. LOUGE and RONALD K. HANSON

*High Temperature Gasdynamics Laboratory, Mechanical Engineering Department,
Stanford University, Stanford, California 94305*

Abstract

Mixtures of cyanogen and nitrous oxide diluted in argon were shock-heated to measure the rate constants of



A broad-band mercury lamp was used to measure CN in absorption at 388 nm [$B^2\Sigma^+(v=0) \leftarrow X^2\Sigma^+(v=0)$], and the spectral coincidence of a CO infrared absorption line [$v(2 \leftarrow 1)$, $J(37 \leftarrow 38)$] with a CO laser line [$v(6 \rightarrow 5)$, $J(15 \rightarrow 16)$] was exploited to monitor CO in absorption. The CO measurement established that reaction (3) produces CO in excited vibrational states. A computer fit of the experiments near 2000 K led to

$$k_2 = 10^{11.70(\pm 0.25, -0.19)} \text{ cm}^3/\text{mol} \cdot \text{s}$$

$$k_3 = 10^{13.26 \pm 0.26} \text{ cm}^3/\text{mol} \cdot \text{s}$$

An additional measurement of NO via infrared absorption led to an estimate of the ratio k_5/k_6 :



with $k_5/k_6 = 10^{3.36 \pm 0.27}$ at 2150 K. Mixtures of cyanogen and oxygen diluted in argon were shock heated to measure the rate constant of



and the ratio k_5/k_6 by monitoring CN in absorption. We found near 2400 K:

$$k_4 = 10^{12.68(\pm 0.27, -0.19)} \text{ cm}^3/\text{mol} \cdot \text{s}$$

and

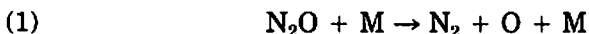
$$k_5/k_6 = 10^{2.69 \pm 0.28}$$

The combined measurements of k_5/k_6 lead to $k_5/k_6 = 10^{-3.07} \exp(+31,800/T)$ ($\pm 60\%$) for $2150 \leq T \leq 2400$ K.

Introduction

Fuel-nitrogen chemistry plays an important role in the formation of combustion-generated nitric oxide. Although the essential features of the kinetic mechanism are commonly agreed upon [1], the values of individual reaction rate constants are not well established [2]. Cyano species such as CN and NCO have been shown to play a key role in this mechanism [1]. In this study, a shock tube was used to measure the rate constants of important reactions involving these radicals at high temperatures.

In order to simplify the reaction mechanism and minimize interfering reactions, mixtures of gases containing only three atoms (C, N, and O) were shock-heated. One mixture was composed of N_2O and C_2N_2 diluted in argon. This mixture is useful for determining the rate constants of reactions (2) and (3), the rate constant for (1) already being well established:



Another mixture contained O_2 and C_2N_2 diluted in argon. If k_2 and k_3 are known, this mixture can yield a value for k_4 and an estimate of k_5/k_6 :



Direct determinations of the above rate constants at flame temperatures are limited. Shaub [3] determined k_3 using a single-pulse shock tube with analysis by gas chromatography. Mulvihill and Phillips [4] conducted a flame study using $H_2-N_2-O_2-C_2N_2$ mixtures and followed the reaction with a mass spectrometer to infer k_4 . Many authors, however, have studied k_2 , k_3 , and k_4 at lower temperatures. Their techniques and results have been extensively reviewed by Baulch et al. [2].

In this paper the experimental facility and optical diagnostics will first be described, then the data reduction and the results for each of the mixtures will be presented.

Experimental

The experiments were conducted in a 15.2-cm internal diameter stainless-steel pressure-driven shock tube [5]. Shock speeds varied

between 1.37 and 1.79 mm/ μ s, with attenuation of 0.5%/m or less. Typical leak plus outgassing rates were $1-3 \times 10^{-5}$ torr/min. Gases were taken directly from commercial cylinders (Matheson) with the following purities: O₂ and N₂O (>99.9%); C₂N₂ (0.95% diluted in argon; HCN and CNCl < 50 ppmv, O₂ < 20 ppmv, CO₂ < 20 ppmv). The shock-tube test section and optical diagnostic systems for CO and CN are shown schematically in Figure 1. The signals obtained from these diagnostics were acquired by a digital oscilloscope (Nicolet Explorer III, dc coupled through a 100-kHz upper frequency cutoff filter) and stored on tape using a computer interface for further data reduction.

CN Absorption System

The absorption from the [$B^2\Sigma^+(v=0) \leftarrow X^2\Sigma^+(v=0)$] band of CN at 388 nm was used as a CN diagnostic. The system consisted of a high-pressure broad-band Hg lamp (Oriol, 200 W), focusing optics, a 0.3-m monochromator, and a photomultiplier tube (RCA 1P28A) with a 6-k Ω load resistor.

The monochromator (Instruments S.A., holographic grating blazed at 250 nm) was calibrated using a Hg spectral lamp (Oriol) and an

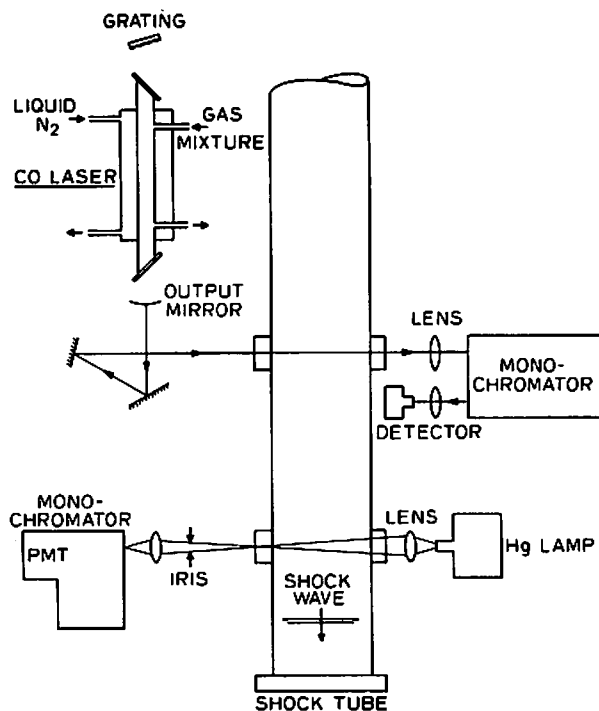


Figure 1. Shock tube *in situ* CN and CO diagnostics.

Ar⁺ laser. The entrance and exit slit widths were measured to be 190 and 103 μm by recording a scan of the slit function under illumination from a He-Ne laser. An iris was used to block extraneous CN emission (see Figure 1). Although the lamp blackbody temperature was always higher than the experimental heat bath, it was discovered from separate measurements that CN emission exceeded that expected for electronic equilibrium. This confirmed, under our experimental conditions, the findings of Setser and Thrush [6]. In fact, the detected signal may be as much as 1000 times higher than the equilibrium CN emission for the $\text{N}_2\text{O}-\text{C}_2\text{N}_2-\text{Ar}$ mixtures and 50 times for the $\text{O}_2-\text{C}_2\text{N}_2-\text{Ar}$ mixtures. In order to find the upper temperature for emission-free experiments, we conducted a few tests with the Hg lamp blocked. We found that the nonequilibrium emission could be neglected below 2100 K for the $\text{N}_2\text{O}-\text{C}_2\text{N}_2-\text{Ar}$ mixtures and below 2450 K for the $\text{O}_2-\text{C}_2\text{N}_2-\text{Ar}$ mixtures.

A computer program to predict the CN transmission under specified conditions was written in a manner similar to that reported by Colket [7]. Spectroscopic constants for CN were taken from various sources [26-31]. The position, strength, and shape of each line seen by the photomultiplier were computed to generate an absorption coefficient profile $\beta(\lambda)$ as a function of wavelength:

$$\beta(\lambda) = \sum_{\text{lines}} \left(\frac{\pi e^2}{m_e c^2} \right) \frac{(2J'' + 1) \exp\{- (hc/kT)[T_e(n'') + G(v'') + F(J'')]\}}{Q_e Q_v Q_r} \\ \times \frac{N}{RT} f_{\text{el}} q_{v'v''} \frac{S_{J'J''}}{2J'' + 1} \phi(\lambda - \lambda_0) \text{cm}^{-1} \cdot \text{atm}^{-1}$$

where $T_e(n'')$, $G(v'')$, and $F(J'')$ are the electronic, vibrational, and rotational energies of the lower state (cm^{-1}); R is the universal gas constant ($\text{atm} \cdot \text{cm}^3/\text{mol} \cdot \text{K}$); N is Avogadro's number; f_{el} , $q_{v'v''}$, and $S_{J'J''}$ are the oscillator strength, the Franck-Condon factor, and the rotational line strength, respectively; Q_e , Q_v , and Q_r are the electronic, vibrational, and rotational partition functions; and $\phi(\lambda - \lambda_0)$ is the lineshape factor (cm). The quantity $\pi e^2/m_e c^2 = 8.826 \times 10^{-13} \text{ cm}$. The monochromator slit function $M(\lambda)$ and the lamp spectral intensity $P(\lambda)$ were then integrated to obtain the predicted transmission:

$$\frac{I}{I_0} = \frac{\int P(\lambda)M(\lambda) \exp[-\beta(\lambda)P_{\text{CN}}L] d\lambda}{\int P(\lambda)M(\lambda) d\lambda}$$

The computer program was used to relate the experimental transmission traces to the actual CN time history. This procedure is necessary since CN is a strong absorber and in most experiments the gas is not optically thin.

Calibration experiments were performed by shock-heating C_2N_2 and Ar. Partial equilibrium of reaction (8) was assumed and the CN plateau was used as a reference:



A significant uncertainty in the heat of formation of CN prompted us to run these experiments at a relatively high temperature, where conversion of C_2N_2 to CN was virtually complete. Typical conditions were $0.31 \leq p_2 \leq 0.36$ atm, $2890 \leq T_2 \leq 3150$ K, $150 \leq \chi_{\text{CN}} \leq 197$ ppmv. The monochromator wavelength setting was fine-tuned by running experiments with slightly different settings; the position that produced the maximum absorption was retained. (The theory predicts this setting to be 3883 Å for our spectral bandpass, about 2.4 Å.)

Since we used known CN spectroscopic parameters, a calibration was in principle superfluous. However, small errors in the monochromator dial position and slit function could have a significant effect on the actual transmission. The calibration runs were thus aimed at establishing an "effective" value for the oscillator strength f_{el} , which could later be used to extrapolate transmission calculations to other conditions. The quantity was found to be 0.024, which is within the range of the literature values [26]. The experimental scatter was less than 6%, which implies an equal uncertainty in the inferred CN concentration.

Additional uncertainties in [CN] are due to the lamp noise ($\approx 7\%$) and to the error introduced by extrapolating the calibration to conditions outside the range of calibration ($\leq 15\%$). The three uncorrelated [CN] uncertainties mentioned above may be combined to give a global calibration uncertainty of $[\Sigma(\text{uncertainty})^2]^{1/2} = \pm 18\%$.

CO Laser Absorption System

The CO laser system is sketched in Figure 1. It is composed of a liquid-nitrogen-cooled continuous-wave electric discharge CO laser, aligning and focusing optics, a monochromator (Jarrell-Ash, 0.5 m, 4 μm grating) and a fast (1- μs) InSb infrared detector (Judson J-10, with Perry 720 preamplifier). The laser has been described by Hanson et al. [8]. The grating (blazed at 5.2 μm) enables tuning of the output beam to the desired CO line. The monochromator is used to remove adjacent interfering laser lines. This diagnostic takes advantage of certain spectral coincidences between high-lying CO laser lines and lower lying CO absorption lines. Only two such coincidences were found in the spectral range of our laser (Table I). The quantity δ is the spacing between the laser line and the CO absorption line center. Both choices provide an absorption diagnostic sensitive to the CO population in the first vibrational state $v'' = 1$.

The first coincidence (1948 cm^{-1}) was used, because it provided better detection limits and more reliable lasing conditions. Calibration runs were performed to measure $2\gamma(300 \text{ K})$, the collision width per

TABLE I. CO—CO coincidences.

CO laser line [9]		CO absorption line ^a		non-resonance δ	CO($v=1$) line strength (2000°K) ^b
transition	$\nu(\text{cm}^{-1})$	transition	$\nu(\text{cm}^{-1})$	cm^{-1}	$\text{cm}^{-2}\text{atm}^{-1}$
$\nu(6+5)$ J(15+16)	1948.7274	$\nu(2+1)$ J(37+38)	1948.7429	0.0155	$6.18 \cdot 10^{-2}$
$\nu(9+8)$ J(6+7)	1907.6872	$\nu(2+1)$ J(45+46)	1907.6765	0.0107	$2.90 \cdot 10^{-2}$

^a Extrapolated to $J = 38$ from Todd et al. [9], using their Dunham coefficients.

^b Using the experimental band strength at 273.2 K of $282 \text{ cm}^{-2} \cdot \text{atm}^{-1}$ [10].

unit pressure, which is needed to calculate the Voigt absorption line-shape factor for the high-temperature experiments. Knowledge of $2\gamma(300 \text{ K})$ and the CO($v = 1$) line strength is sufficient to calculate (using Beer's law) the concentration of CO($v = 1$) from a transmission measurement at known pressure and temperature [8,10]. Mixtures of CO and Ar were shock-heated under the following conditions: $2040 \text{ K} \leq T_2 \leq 2430 \text{ K}$, $0.58 \leq p_2 \leq 0.70 \text{ atm}$, CO—Ar ≈ 2 –98. We assumed here the temperature dependence that Hanson [11] had determined for the P(11) line, namely, $2\gamma(300 \text{ K}) = 2\gamma(T)(T/300)^{0.73}$, and we found $2\gamma(300 \text{ K}) \approx 0.10 \pm 0.03 \text{ cm}^{-1} \cdot \text{atm}^{-1}$. This value is in good agreement with the recent findings of Varghese and Hanson [10,11].

Kinetics Experiments

Seven runs were conducted with mixtures of $\text{N}_2\text{O}-\text{C}_2\text{N}_2-\text{Ar} \approx 12$ –3–985 and conditions in the range $0.67 \leq p_2 \leq 0.75 \text{ atm}$, $1920 \leq T_2 \leq 2110 \text{ K}$, $3.51 \leq \rho_{21} \leq 3.61$. (ρ_{21} is the density ratio across the shock and also the ratio of particle time to laboratory time.) Four runs were conducted with mixtures of $\text{O}_2-\text{C}_2\text{N}_2-\text{Ar} \approx 6$ –6–988 and $0.56 \leq p_2 \leq 0.61 \text{ atm}$, $2320 \leq T_2 \leq 2450 \text{ K}$, $3.62 \leq \rho_{21} \leq 3.65$. In both the $\text{N}_2\text{O}-\text{C}_2\text{N}_2$ and the $\text{O}_2-\text{C}_2\text{N}_2$ mixtures, spontaneous emission considerations in the CN absorption system placed an upper bound on the temperature. The lower bound on temperature was set by reaction-rate and detection-limit considerations. The first mixture ($\text{N}_2\text{O}-\text{C}_2\text{N}_2-\text{Ar}$) used excess N_2O to minimize interferences from reactions other than (2) and (3); however, the initial $[\text{N}_2\text{O}]/[\text{C}_2\text{N}_2]$ ratio was kept below 4.5 to avoid excessive N_2O background absorption (see below) and possible production of undesirable radicals such as NCN (see Drummond [16]). The C_2N_2 level in both mixtures was adjusted to ensure an optimum sensitivity of the absorption system in measuring the peak value of [CN].

N₂O–C₂N₂–Ar Mixtures—Analysis and Results

Reaction Mechanism. The complete reaction mechanism utilized is shown in Table II, but a simplified description can be given as follows. At early times, N₂O rapidly decomposes to provide O atoms; C₂N₂ then reacts to form CN, which in turn is removed by O atoms to give CO:



After a brief induction time, the slope of the [CN] time history is nearly proportional to k_2 :

$$\frac{d[\text{CN}]}{dt} = k_2[\text{C}_2\text{N}_2][\text{O}]$$

TABLE II. Reaction mechanism.

Reactions	ΔH^a	equil. const. ^b	rate constants ^c			Source (Ref #)
			$\log_{10} A$	m	θ (°K)	
N ₂ O+M→N ₂ +O+M	+40	-2.5	23.89	-2.5	32710	[19]
C ₂ N ₂ +O→CN+NCO	+5	0.2	12.66	0	4440	This study
CN+O→CO(v=1)+N	-71	7.0	13.31	0	210	This study
CN+O ₂ →NCO+O	-3	0.3	12.75	0	0	This study
NCO+O→CO+NO	-106	11.5	13.00	0	0	[20] ^d
NCO+M→N+CO+M	+48	-4.2	13.00	0.5	20630	[7] ^d
CO(v=1)+N→CO+M	-6	0.7	-5.81	4.6	3610	[18]
C ₂ N ₂ +M→CN+CN+M	+131	-11.6	34.46	-4.5	63150	[21]
N ₂ O+O→NO+NO	-39	5.7	13.84	0	13400	[19]
N ₂ O+O→N ₂ +O ₂	-82	9.1	14.00	0	14100	[19]
N ₂ +O→N+NO	+75	-7.6	14.26	0	38370	[19]
NO+O→N+O ₂	+32	-4.2	9.58	1.0	20820	[19]
NCO+N→N ₂ +CO	-181	19.1	13.30	0	0	[20]
NCO+N→CN+NO	-29	3.8	14.66	0	6540	[7] ^e

^a Heat of reaction at 2000 K (kcal/mol) [32].

^b $\log_{10}(k_{\text{forward}}/k_{\text{backward}})$ at 2000 K.

^c Using the notation $k = AT^m \exp(-\theta/T)$ cm³/mol · s.

^d These values for k_5 and k_6 result in a lower value of k_5/k_6 than found in this study.

^e Colket measured $k_{\text{backward}} = 10^{14} \exp(-21,190/T)$ cm³/mol · s; we assumed $k_f/k_b = 4.54 \exp(14,650/T)$.

At the peak of the CN trace,

$$\frac{d[\text{CN}]}{dt} \approx k_2[\text{C}_2\text{N}_2][\text{O}] - k_3[\text{CN}][\text{O}] = 0$$

and hence

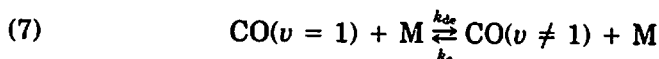
$$\frac{[\text{CN}]^{\text{peak}}}{[\text{C}_2\text{N}_2]} = \frac{k_2}{k_3}$$

The [CN] peak value thus depends primarily on the ratio k_2/k_3 , and the early-time behavior depends on k_2 . A record of [CN] is therefore sufficient to infer k_2 and k_3 .

Experimental Fit

A numerical routine derived from the NASA-Lewis general chemical kinetics program [17] incorporating the mechanism in Table II was used for the kinetics calculations. The calculated CN concentrations were numerically converted into transmission profiles for comparison with the experimental traces.

To interpret the CO absorption records, the vibrational relaxation (about 500- μ s particle time for $p_2 = 0.7$ atm and $T_2 = 2000$ K) was modeled using the following excitation/deexcitation process:



where $\text{CO}(v \neq 1)$ represents all vibrational states but $v = 1$. It can be shown that

$$\frac{k_e}{k_{de}} \equiv \frac{[\text{CO}(v = 1)]^*}{[\text{CO}(v \neq 1)]^*} = \frac{\exp(-\theta_{\text{vib}}/T)}{Q_{\text{vib}} - \exp(-\theta_{\text{vib}}/T)}$$

and

$$p\tau(v = 1) = RT/(k_e + k_{de})$$

where τ is the vibrational relaxation time from $v = 1$; θ_{vib} is the vibrational temperature = $hc\omega_e/k$; Q_{vib} is the vibrational partition function; and the asterisk * refers to equilibrium conditions. We used Millikan and White's [18] results for $p\tau$ (which agreed within 16% with our own measurements conducted in CO-Ar mixtures with $1800 \leq T_2 \leq 2900$ K). From the above expressions, k_e and k_{de} were extracted and fitted to Arrhenius expressions for use in the kinetics modeling.

In all kinetics experiments a background absorption of the CO laser was observed that we attributed to N_2O . Accordingly, we calculated the absorption spectrum of N_2O in the vicinity of the CO laser lines [12-15] for a temperature of 2000 K. At this temperature N_2O has a

large number of high-level ν_3 subbands which might produce the observed background interference. We estimate that many lines of strengths up to $0.001 \text{ cm}^{-1} \cdot \text{atm}^{-1}$ are present in this spectral region, and assuming reasonable broadening parameters, the initial background absorption can be as much as 0.6% under typical conditions. This is consistent with our experimental observations. The $\text{CO}(v = 1)$ theoretical profiles were numerically converted to fractional transmission and corrected for the N_2O absorption background prior to comparison with the actual experimental traces.

Figure 2 shows a best computer fit (solid lines) to the CN and CO traces simultaneously recorded in one experimental run. The error bars correspond to the calibration uncertainties, namely, $\Delta[\text{CN}]/[\text{CN}] = \pm 18\%$ for CN and $\Delta[2\gamma(300\text{K})] = 0.03 \text{ cm}^{-1} \cdot \text{atm}^{-1}$ for CO. The dotted line that appears on the CO record is a computer prediction which assumes that reaction (3) produces CO in the ground vibrational state. In this case, according to the model, $\text{CO}(v = 1)$ would barely absorb any incoming laser radiation at the early stages of the experiment, since its relaxation is very slow. We conclude therefore that reaction (3) produces CO in excited vibrational states; the quality of

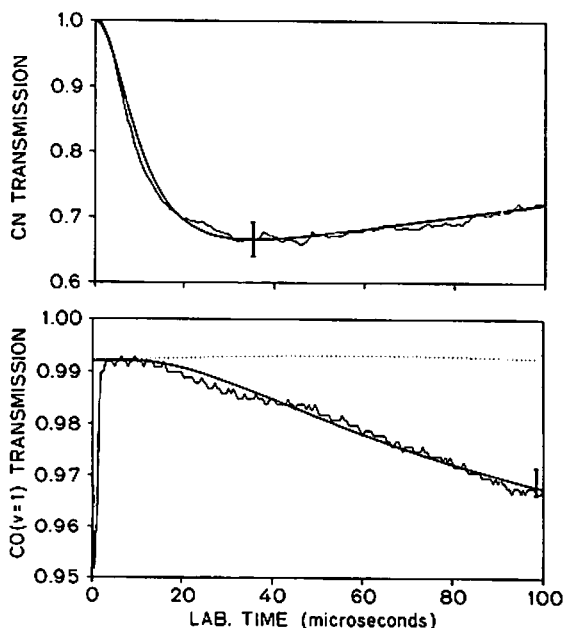


Figure 2. Conditions— $T_2 = 1943 \text{ K}$, $p_2 = 0.67 \text{ atm}$, $\text{N}_2\text{O}-\text{C}_2\text{N}_2-\text{Ar} \approx 12-3-985$. Solid line—best computer fit using $k_2 = 10^{11.67}$, $k_3 = 10^{13.26} (\text{cm}^3/\text{mol} \cdot \text{s})$, and other rates shown in Table II. Dotted line—computer-generated profile assuming $\text{CN} + \text{O} \rightarrow \text{CO}(v = 0) + \text{N}$.

the fit further suggests that $\text{CO}(v = 1)$ is the principal product of this reaction. For a more detailed discussion of the products of reaction (3) at room temperature, the reader is directed to the paper by Schmatjko and Wolfrum [22].

Discussion and Results

For the $\text{N}_2\text{O}-\text{C}_2\text{N}_2-\text{Ar}$ mixtures, the peak $[\text{CN}]$ value is nearly proportional to the ratio k_2/k_3 . The uncertainty in the fit to the peak is therefore also the uncertainty in k_2/k_3 . Figure 3 shows the influence of varying k_2/k_3 in the kinetic calculation by $\pm 18\%$ (the overall calibration uncertainty for $[\text{CN}]$; see Table III).

For a fixed k_2/k_3 ratio, the shape of the CN trace is dependent on the specific values of k_2 and k_3 . The uncertainty in k_2 and k_3 (associated with the fitting process) is thus determined by the range of values that produce an acceptable fit. Figure 4 shows the sensitivity of the fit to excursions of both k_2 and k_3 , with the ratio k_2/k_3 fixed. The $+50\%$ excursion particularly affects the time to peak and the fit after $40 \mu\text{s}$. Larger excursions clearly would not provide an acceptable fit. The -30% excursion fails to reproduce the initial slope. Note that these excursions produce equally unacceptable fits of the $\text{CO}(v = 1)$ trace. Conservative minimum uncertainties in k_2 and k_3 are therefore $+50\%$, -30% (see "uncertainty in the fit" in Table III).

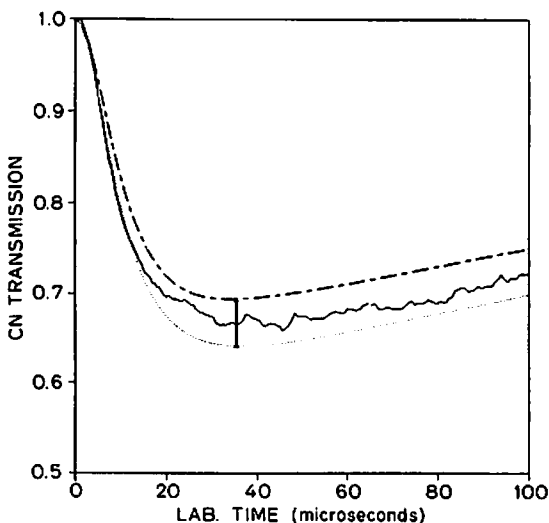


Figure 3. Conditions—same as Figure 2. Dotted lines—computer-generated profiles using best rates except (\cdots), k_2/k_3 ($+20\%$); ($-\cdot-$), k_2/k_3 (-20%).

TABLE III. Uncertainties.

Reactions	Uncertainty factors	Ref.	effect on:		
			k_2	k_3	k_2/k_3
$N_2O+M \rightarrow N_2+O+M$	1.22	[19]	-18%	-18%	0%
	0.82		+18%	+18%	0%
$NCO+O \rightarrow CO+NO$	10.0		0%	-4%	+4%
	0.1		0%	+4%	-4%
$NCO+M \rightarrow N+CO+M$	10.0		0%	-8%	+8%
	0.1		0%	+8%	-8%
$CN+N \rightarrow C+N_2^a$	1.45		-12%	-40%	+18%
calibration	+18%		-9%	+9%	-18%
uncertainty	-18%		+9%	-9%	+18%
uncertainty			+50%	+50%	0%
in the fit			-30%	-30%	0%
exp. scatter			-20% +20%	-20% +20%	-20% +20%
total uncertainty ^b = $[\sum(\text{uncert.})^2]^{1/2}$			-43% +57%	-58% +58%	-28% +34%

^a This reaction was introduced in the mechanism with $k = (4.4 \pm 2) = 10^{14} \exp(-4530/T) \text{ cm}^3/\text{mol} \cdot \text{s}$ [23].

^b The individual uncertainties are statistically independent.

Additional uncertainties in k_2 and k_3 may result from uncertain knowledge of other rates of reactions present in the mechanism. In order to estimate these uncertainties, individual rates (Table II) were adjusted by reasonable factors (based on current literature or our judgment); k_2 and k_3 were subsequently modified to ensure the return to an optimum fit. Table III summarizes the uncertainty analysis. The reaction $CN + N \rightarrow C + N_2$ was introduced as a possible interference to the proposed mechanism, although there is considerable question regarding its rate constant (see Baulch et al. [2]). Note that, according to our fitting method, k_2 and k_3 are dependent quantities (e.g., the uncertainty in k_1 produces equal uncertainties in k_2 and k_3 ; see Table III). As a consequence, the relative uncertainty in the ratio k_2/k_3 is less than the sum of the respective uncertainties in k_2 and k_3 .

On the basis of this analysis, we recommend at temperatures near 2000 K:

$$k_2 = 10^{11.70(+0.25, -0.19)} \text{ cm}^3/\text{mol} \cdot \text{s}$$

$$k_3 = 10^{13.26 \pm 0.26} \text{ cm}^3/\text{mol} \cdot \text{s}$$

and

$$k_2/k_3 = 10^{-1.56(+0.15, -0.12)}$$

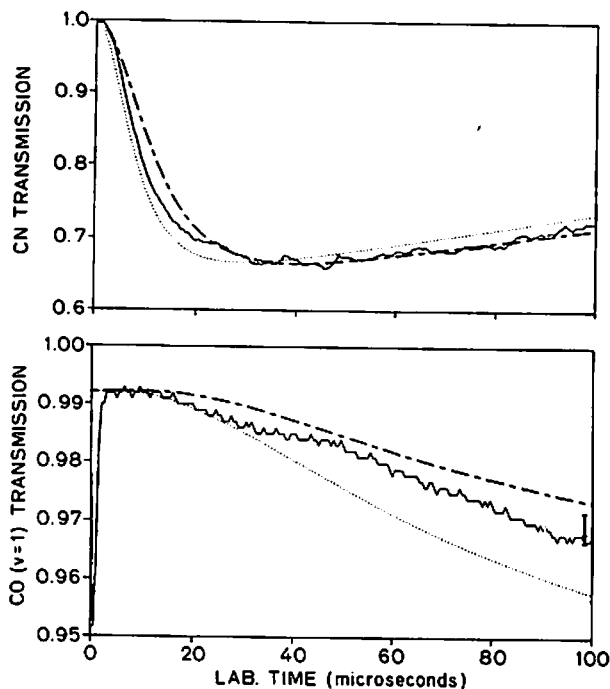


Figure 4. Conditions—same as Figure 2. Dotted lines—computer-generated profiles using best rates except (\cdots) k_2 and k_3 (+50%); ($-\cdot-$), k_2 and k_3 (-30%).

No noticeable temperature dependence was observed in the limited range of these experiments ($1920 \leq T \leq 2110$ K).

Our measurement of k_2 is plotted in Figure 5 along with the result of Boden and Thrush [25] (shown with error bars recommended by Baulch et al. [2]). An activation energy of 8.8 ± 2.0 kcal/mol can be deduced assuming a straight-line fit (labeled "this evaluation") to the high- and low-temperature data. This is reasonably consistent with the heat of reaction at 2000 K, $\Delta H \approx +5$ kcal/mol.

Figure 6 shows our result for k_3 plotted on the compilation of Baulch et al. [2]. As expected for this exothermic reaction, the activation energy of k_3 is low. An accurate determination of this activation energy is prohibited by the size of our error bars and the scatter of low-temperature data. For our detailed kinetics modeling, we used a simple straight-line fit (labelled "this evaluation") to our data at 2000 K and the room-temperature recommendation of Baulch et al. [2].

In a few experiments, the CO laser diagnostic was tuned to coincidence with an $\text{NO}(v=0)$ absorption line (Λ - doublet) (laser line: $v(7 \rightarrow 6)$, $J(12 \rightarrow 13)$, see Hanson et al. [8]). Vibrational equilibrium

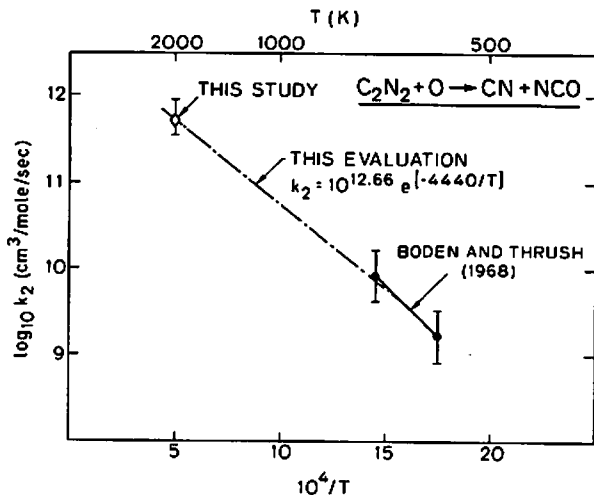


Figure 5. Arrhenius plot for k_2 . Note that - - - is an Arrhenius fit to the high- and low-temperature data.

of NO was assumed, even though there is some evidence for NO production in excited vibrational states (see Basco [24]). An NO transmission record, corrected for N_2O absorption, was calculated using the computer-generated NO profile and compared with the experimental trace. Modeling shows that the NO profile is reasonably sensitive to the ratio k_5/k_6 , with larger values of k_5 producing more NO. On the

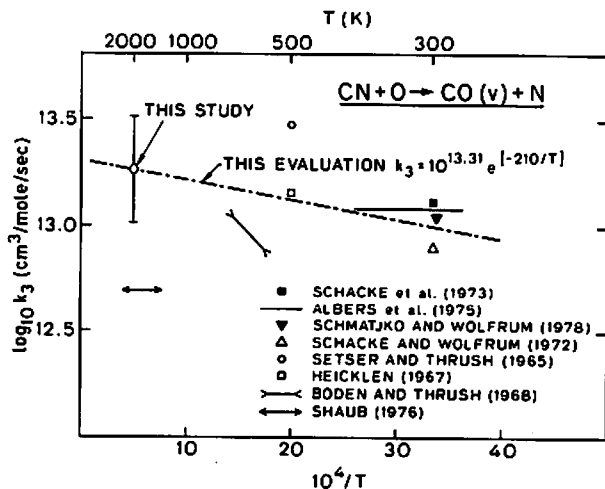


Figure 6. Arrhenius plot for k_3 .

contrary, larger values of k_6 lead to increased levels of N atoms, which in turn remove NO by reaction (11):



Figure 7 shows the computer fit (solid line) using $k_2 = 10^{11.56} \text{ cm}^3/\text{mol} \cdot \text{s}$, $k_3 = 10^{13.08} \text{ cm}^3/\text{mol} \cdot \text{s}$, and $k_5/k_6 \approx 10^{3.36 \pm 0.27}$ for $T_2 = 2150 \text{ K}$. The dashed line is the computer fit obtained by assuming literature values for k_5 and k_6 (see Table II), and the set of rate constants which would, within reasonable bounds, predict the largest production of NO. It is clear that the literature-based value for k_5/k_6 [7,20] cannot fit the experimental NO trace and is too low. This observation is confirmed at higher temperatures in our discussion of $\text{O}_2\text{-C}_2\text{N}_2\text{-Ar}$ mixtures.

$\text{O}_2\text{-C}_2\text{N}_2\text{-Ar}$ Mixtures—Analysis and Results

Despite the apparent simplification of this mixture (no N_2O is present), the reaction paths prove to be more complicated. Figure 8 shows a sketch of the global mechanism.

As a first step, C_2N_2 decomposes slowly via reaction (8) to give CN. The latter then reacts immediately with oxygen to form O atoms:

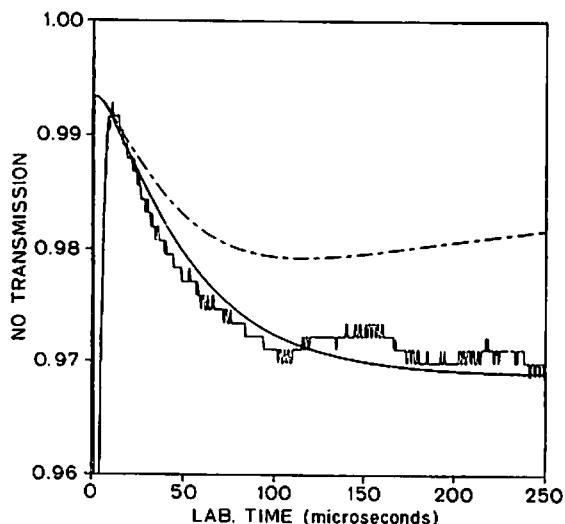


Figure 7. Conditions— $T_2 = 2150 \text{ K}$, $p_2 = 0.65 \text{ atm}$, $\text{N}_2\text{O-C}_2\text{N}_2\text{-Ar} \approx 12\text{-}3\text{-}985$. Solid line—best computer fit to the trace using $k_2 = 10^{11.56}$, $k_3 = 10^{13.08} \text{ cm}^3/\text{mol} \cdot \text{s}$, $k_5/k_6 = 10^{3.36}$, and other rates shown in Table II. Dotted line—computer-generated profile assuming $k_5/k_6 = 10^{2.50}$ (literature values) and k_2, k_3 as above.

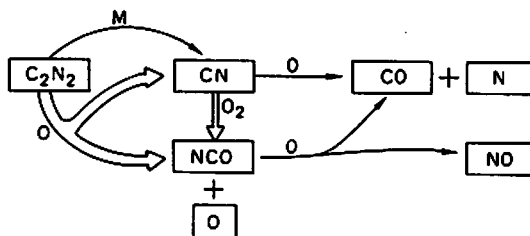


Figure 8. Reaction paths for C_2N_2 - O_2 -Ar mixtures.

As soon as they are produced, the O atoms provide a sink for C_2N_2 via reaction (2). As the chemistry proceeds, more O atoms are available to attack CN [reaction (3)] or NCO [reaction (5)]. O atoms obviously play a critical role in this system, and any reaction involving them can affect the history of all species, including CN. With an overall mechanism that allows little simplification, a computer fitting technique proves necessary.

Figure 9 shows a best computer fit (solid line) to an experimental trace. The dotted lines illustrate the dependence of the fit on k_4 . It appears that increasing or decreasing k_4 generates a parallel fit which retains a similar overall shape.

Using our computer model, we showed that an increase in k_5 or a decrease in k_6 (and conversely) produced equivalent variations in the

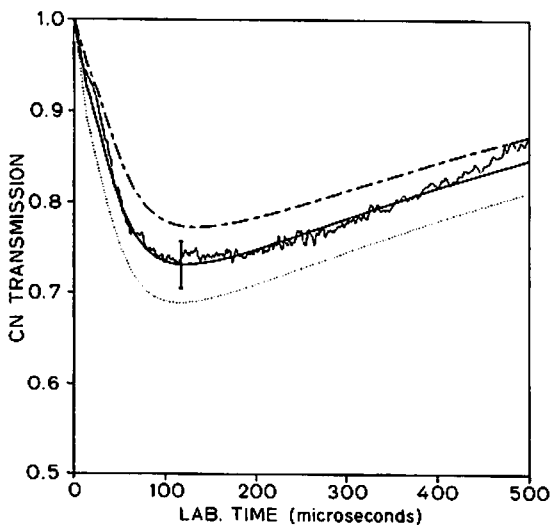


Figure 9. Conditions— $T_2 = 2315$ K, $p_2 = 0.61$ atm, O_2 - C_2N_2 -Ar = 6-6-988. Solid line—best computer fit using $k_4 = 10^{12.70}$ $cm^3/mol \cdot s$, $k_5/k_6 = 10^{2.93}$ and other rates shown in Table II. Dotted lines—computer-generated profiles using best rates except (\cdots), k_4 (-60%); ($-\cdot-$), k_4 (+60%).

predicted CN profile. The fit therefore depends on the ratio k_5/k_6 . Furthermore, we found that this ratio, unlike k_4 , controls not only the peak CN value, but also the shape of the fit, especially at late times. This effect is due to the critical role of O atoms mentioned above. If k_5 is large, reaction (5) consumes O atoms to a greater extent, thus preventing a faster decay of CN by reaction (3). An equivalent situation arises from a small k_6 . In this case, NCO levels are increased, reaction (5) becomes the preferential NCO removal path, and O atom consumption via reaction (5) is again increased. Note that the opposite effect (acceleration of the CN decay) would conversely be obtained through a smaller k_5 or a larger k_6 .

It therefore appears possible to determine k_4 and k_5/k_6 by fitting the CN trace alone: a unique set of values for k_4 and k_5/k_6 can fit both the slope of the CN decay (influenced by k_5/k_6) and the peak CN concentration (influenced by k_5/k_6 and k_4). Figure 10 illustrates the effect of k_5/k_6 on the slope of the CN decay.

In order to estimate the uncertainties in these determinations, we constructed Table IV in a fashion similar to that used in our analysis of $N_2O-C_2N_2-Ar$ mixtures. An important feature of this table is the influence of our previous uncertainties in k_2 and k_3 . If we assume a known ratio k_2/k_3 , most of the uncertainty in k_2 and k_3 is translated into a similar uncertainty in k_5/k_6 . This effect is illustrated in Figure 11. Here k_2 , k_3 , and k_5/k_6 are simultaneously varied by $\pm 40\%$. The

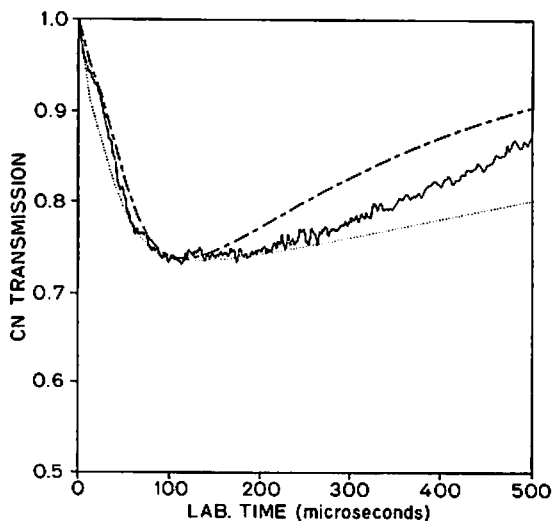


Figure 10. Conditions—same as Figure 9. Dotted lines—computer-generated profiles using best rates except (· · ·), k_5/k_6 (+60%) and k_4 (-34%); (- - -), k_5/k_6 (-60%) and k_4 (+56%).

TABLE IV. Uncertainties.

Reactions	Uncertainty factors	Ref.	effect on:	
			k_4	k_5/k_6
$C_2N_2+M \rightarrow 2CN+M$	1.67 (a)	[21]	+18%	+8%
	0.60		-11%	0%
$C_2N_2+O \rightarrow CN+NCO$ and (b)	+58%		+13%	+58%
$CN+O \rightarrow CO+N$	-58%		+24%	-58%
$NCO+N \rightarrow CN+NO$	10.0		+30%	0%
$NCO+N+N_2+CO$	10.0		-11%	-26%
calibration	+18%		+37%	0%
uncertainty	-18%		-37%	0%
exp. scatter			-18% +18%	-15% +15%
total uncertainty = $[\Sigma(\text{uncert.})^2]^{1/2}$			-44% +61%	-65% +60%

^a This rate controls the early CN slope and could be adjusted accordingly.

^b Both k_2 and k_3 were equally modified.

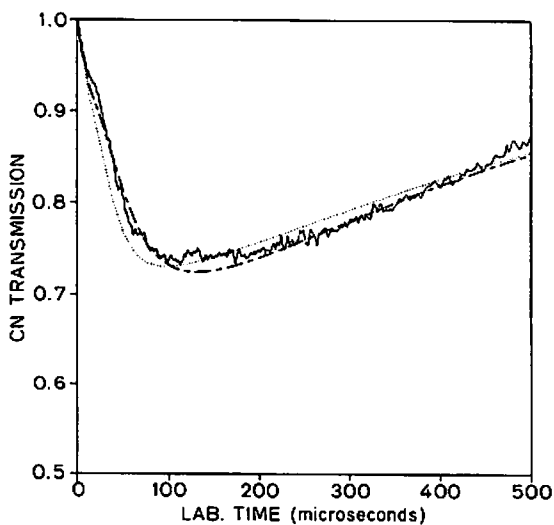


Figure 11. Conditions—same as Figure 9. Dotted lines—computer-generated profiles using best rates except (\cdots), k_2 and k_3 (+40%); k_5/k_6 (+40%); ($-\cdot-$), k_2 and k_3 (-40%); k_5/k_6 (-40%).

result of those excursions still appears as a reasonable fit. Thus any variation in (k_2, k_3) can approximately be offset by the same variation in k_5/k_6 .

Our inferred values for k_4 and k_5/k_6 at temperatures near 2400 K are

$$k_4 = 10^{12.68(+0.27, -0.19)} \text{ cm}^3/\text{mol} \cdot \text{s}$$

and

$$k_5/k_6 = 10^{2.69 \pm 0.28}$$

This value of k_5/k_6 at 2400 K is higher than the literature estimate by at least a factor of 2. However, the suggested temperature dependence of this ratio based on our determinations at 2150 K (see $\text{C}_2\text{N}_2\text{-N}_2\text{O-Ar}$ mixtures) and at 2400 K is consistent with Colket's estimate [7] and the size of our error bars. (Our determination corresponds to a net activation energy of 63 ± 26 kcal/mol; Colket's estimate is 43 kcal/mol at 2300 K.) We recommend $k_5/k_6 = 10^{-3.07} \exp(+31,800/T)$ ($\pm 60\%$) for $2150 \leq T \leq 2400$ K.

Figure 12 is an Arrhenius plot adding our value for k_4 to the review of Baulch et al. [2]. This measurement agrees well with previous work, except for the flame study of Mulvihill and Phillips [4]. Within the scatter of the low- and high-temperature results, the reaction shows no significant temperature dependence. We recommend $k_4 = 10^{12.75(+0.20, -0.15)} \text{ cm}^3/\text{mol} \cdot \text{s}$ over the temperature range $300 \leq T \leq 2400$ K.

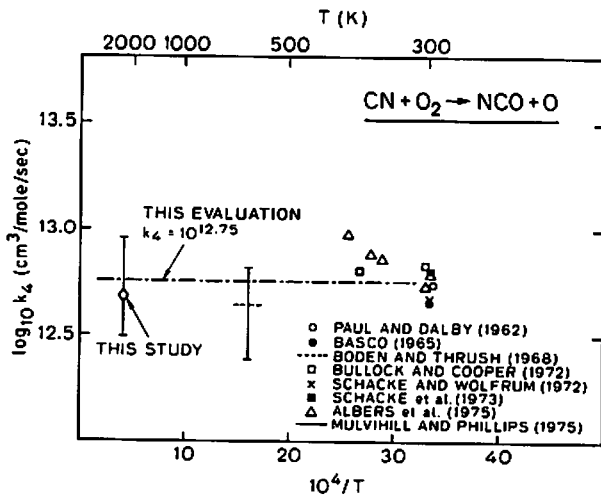


Figure 12. Arrhenius plot for k_4 .

Acknowledgment

This work was supported by the Environmental Protection Agency under Contracts R-810019-01 and R-807942-02, and by the Department of Energy under Contract EY-76-03-0326, PA 68. Useful conversations with M. B. Colket of the United Technologies Research Center and C. T. Bowman of Stanford University are gratefully acknowledged.

Bibliography

- [1] Y. H. Song, D. W. Blair, V. J. Siminski, and W. Bartok, "Eighteenth Symposium (International) on Combustion," The Combustion Institute, Pittsburgh, PA, 1981, p. 53.
- [2] D. L. Baulch, J. Duxbury, S. J. Grant, and D. C. Montague, *J. Phys. Chem. Ref. Data*, **10**, Suppl. 1, 1/576 (1981).
- [3] W. M. Shaub, Ph.D. thesis, Cornell University, Ithaca, NY, 1976.
- [4] J. N. Mulvihill and L. F. Phillips, "Fifteenth Symposium (International) on Combustion," The Combustion Institute, Pittsburgh, PA, 1975, p. 1113.
- [5] J. P. Monat, R. K. Hanson, and C. H. Kruger, *Comb. Sci. Technol.*, **16**, 21 (1977).
- [6] D. W. Setser and B. A. Thrush, *Proc. R. Soc.*, **A288**, 256 (1965).
- [7] M. B. Colket, *Abstr. Papers of the Am. Chem. Soc.*, **183**, Phys., p. 7 (1982).
- [8] R. K. Hanson, J. P. Monat, and C. H. Kruger, *J. Quant. Spectrosc. Radiat. Transfer*, **16**, 705 (1976).
- [9] T. R. Todd, C. M. Clayton, W. B. Telfair, T. K. McCubbin, Jr., and J. Pliva, *J. Mol. Spectrosc.*, **62**, 201 (1976).
- [10] P. L. Varghese and R. K. Hanson, *J. Quant. Spectrosc. Radiat. Transfer*, **26**, 339 (1981).
- [11] R. K. Hanson, "Proceedings of the 11th International Symposium on Shock Tubes and Waves," University of Washington Press, Seattle, WA, 1978, p. 432.
- [12] L. D. Gray Young, *J. Quant. Spectrosc. Radiat. Transfer*, **12**, 307 (1972).
- [13] L. D. Gray Young, *J. Quant. Spectrosc. Radiat. Transfer*, **11**, 1265 (1971).
- [14] J. Pliva, *J. Mol. Spectrosc.*, **25**, 62 (1968).
- [15] J. Pliva, *J. Mol. Spectrosc.*, **27**, 461 (1968).
- [16] L. J. Drummond, *Comb. Sci. Technol.*, **1**, 415 (1970).
- [17] D. A. Bittker and V. J. Scullin, NASA TN D-6586, 1972.
- [18] R. C. Millikan and D. R. White, *J. Chem. Phys.*, **39**, 3209 (1963).
- [19] R. K. Hanson and S. Salimian, in press.
- [20] A. Lifshitz and M. Frenklach, *Int. J. Chem. Kinet.*, **12**, 159 (1980).
- [21] T. Fueno, K. Tabayashi, and O. Kajimoto, *J. Phys. Chem.*, **77**, 575 (1973).
- [22] K. J. Schmatjko and J. Wolfrum, "Sixteenth Symposium (International) on Combustion," The Combustion Institute, Pittsburgh, PA, 1977, p. 819.
- [23] M. W. Slack, *J. Chem. Phys.*, **64**, 228 (1976).
- [24] N. Basco, *Proc. R. Soc.*, **A283**, 302 (1965).
- [25] J. C. Boden and B. A. Thrush, *Proc. R. Soc.*, **A305**, 107 (1968).
- [26] R. G. Bennett and F. W. Dalby, *J. Chem. Phys.*, **36**, 399 (1962).
- [27] I. Kovacs, "Rotational Structure in the Spectra of Diatomic Molecules," Elsevier, New York, 1969.
- [28] G. H. Dieke and H. M. Crosswhite, *J. Quant. Spectrosc. Radiat. Transfer*, **2**, 97 (1962).
- [29] G. Herzberg, "Molecular Spectra and Structure: I. Spectra of Diatomic Molecules," Van Nostrand, Princeton, NJ, 1950.

- [30] A. G. Gaydon, "The Spectroscopy of Flames," Wiley, New York, 1974.
[31] R. Engleman, *J. Mol. Spectrosc.*, **49**, 106 (1974).
[32] "JANAF Thermochemical Tables," 2nd ed., D. R. Stull and H. Prophet, Project Directors, Natl. Bur. Stand., Washington, DC, NBS37, 1971.

Received February 7, 1983

Accepted July 11, 1983